

## Supporting Information

### **To promote sulfur conversion kinetics by a solid auxiliary redox couple embedded in cathode for Li-S batteries**

**Girum Girma Bizuneh, †<sup>1</sup> Jingmin Fan, †<sup>1</sup> Pan Xu,<sup>1</sup> Ruming Yuan,<sup>1</sup> Lin Cao,<sup>2</sup> Mingsen Zheng, \*<sup>1</sup> and Quan-Feng Dong\*<sup>1</sup>**

*<sup>1</sup>State Key Laboratory for Physical Chemistry of Solid Surfaces, Department of Chemistry, College of Chemistry and Chemical Engineering, iChem (Collaborative Innovation Center of Chemistry for Energy Materials), Engineering Research Centre of Electrochemical Technologies of Ministry of Education, Xiamen University, Xiamen 361005, China*

*<sup>2</sup>. Dr. L. Cao*

*China Electronics Standardization Institute*

*Beijing 100007, China*

†These authors contributed equally to this work.

\*Correspondence: qfdong@xmu.edu.cn; mszheng@xmu.edu.cn

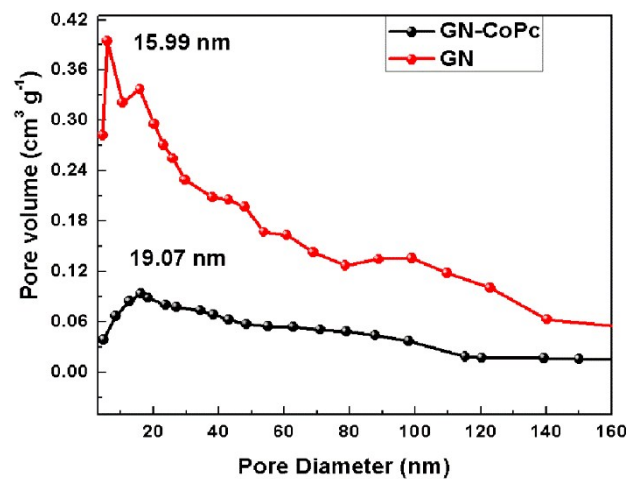


**Fig. S 1. Pore size distribution of GN and GN-CoPc samples determined by the Barret–Joyner–Halenda (BJH) method.**

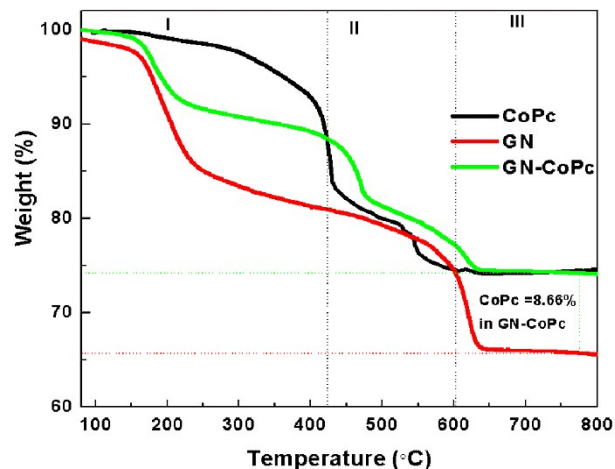


**Fig. S 2. Thermogravimetric weight loss curves of Cobalt phthalocyanine (CoPc), Graphene (GN) and Graphene supported Cobalt phthalocyanine hybrid (GN-CoPc) samples obtained under N<sub>2</sub> atmosphere**

The thermogravimetric measurement of the samples was collected from the room temperature to 800 °C at a temperature ramp of 10°C min<sup>-1</sup> under N<sub>2</sub> atmosphere. The data is presented in (Fig. S2). The weight loss curve as shown in **Fig.S2** can be divided broadly into three zones based on temperature ranges. Zone I (30°C - 400°C), Zone II (400°C - 600°C) and Zone III (600°C - 800°C). In Zone I, both GN and GN-CoPc underwent rapid weight loss as compared with the pristine CoPc. However, the decline in the weight in the case of the GN-CoPc hybrid is not as quick as the one in GN. In Zone I, for the CoPc curve, due to stable CoPc's molecular structure, a very little weight loss was recorded attributed to the residual water vapor<sup>1</sup>. For GN and GN-CoPc hybrid, the residual water loss from the internal of the materials was seen from the 75°C - 165°C <sup>2</sup>. The following crucial weight change was observed between 165°C-238 °C which is ascribed to the thermal decomposition of oxygen-containing functional groups that may be leftover from the reduction steps during synthesis. Zone II represents nearly identical weight loss profiles for GN-CoPc and CoPc samples. Since the CoPc contains nitrogen and hydrogens in its structure, weight loss

observed in the range of 400°C -580 °C represents the partial decomposition of the macrocyclic structure resulting in loss of hydrogen and nitrogen. In such a stage, the decomposition of CoPc yields major products such as cyanogens, hydrogen cyanide, benzonitrile, and phthalonitrile <sup>1, 3, 4</sup>. A similar situation was observed in GN-CoPc, except with the shifting of the temperature ranges to 450°C - 600°C. However, in the case of GN, the absence of nitrogen content in the graphene structure resulted in the similarity between zones (I and II), where an apparently steady weight-loss feature was discerned. In Zone III, the CoPc and GN-CoPc curve shows the residual cobalt metal and carbon left after the complete decomposition of the CoPc and the GN structures. The apparently low weight loss rate at high-temperature ranges of CoPc as well as GN-CoPc hybrid compared to GN implies that the thermal stability of the CoPc and GN-CoPc catalysts. The hybrid GN-CoPc profile can also suggest that the intermediate property attributed from GN and CoPc resulting in a robust framework of GN-CoPc structure with high thermal stability. Moreover, the CoPc content of the GN-CoPc hybrid was determined from the TGA experiment measured under Nitrogen atmosphere. Where the value of 8.66% was obtained by taking the difference in weight loss between GN-CoPc and GN samples at the final temperature region **Fig.S2**.

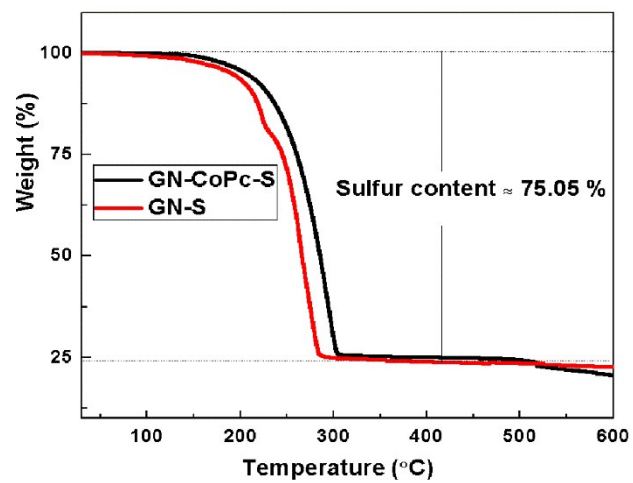


**Fig. S 3.** The thermogravimetric weight loss profiles of the as-prepared cathode composites of GN-CoPc-S and GN-S showing the sulfur content of  $\approx 75.05\%$ . Where, the measurements were performed under  $N_2$  atmosphere

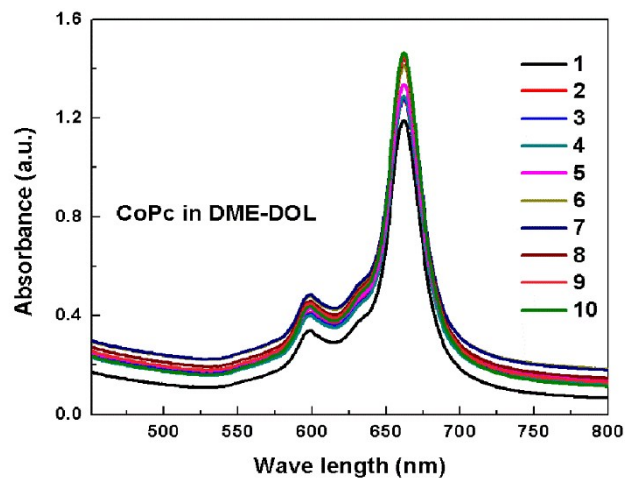


**Fig. S 4. The UV-Vis absorption spectra of ten replicate samples of Cobalt Phthalocyanine in DME-DOL mixed solvent (1:1 v/v).**

In order to determine the maximum saturation concentration of the CoPc in DME-DOL (1:1 v/v)

solvent, the CoPc solution was prepared by adding 0.0286g of CoPc in 5ml of DME-DOL with

sonicating for 2 hrs. Then the clear solution of CoPc was separated from un-dissolved CoPc with centrifugation at 10000 rpm for 5 minutes and the supernatant was preserved for the UV

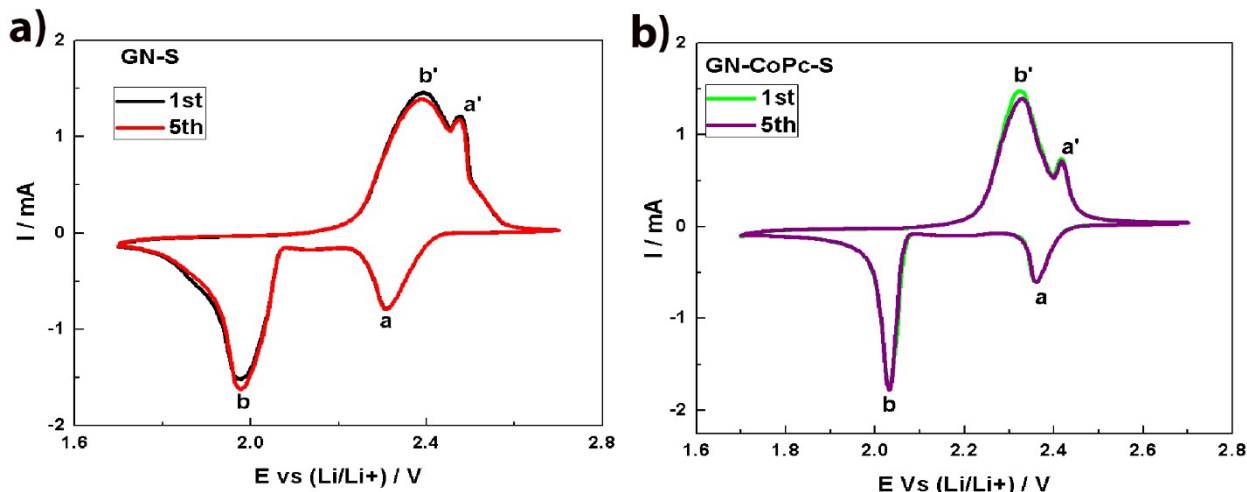


**Fig. S 5. The CV profiles Li-S batteries during the 1<sup>st</sup> and 5<sup>th</sup> cycles of: a) GN-S and b) GN-CoPc-S cathodes showing stable cycle response. The scan rate was 0.1 mV s<sup>-1</sup>.**

measurement. Then the UV-Vis absorption spectra were collected between the wavelength range of 450 nm – 800 wherein this region the Q-band will show the maximum absorption and that will be used to determine the maximum saturation concentration of the CoPc in a given solvent. Accordingly, 10 replicate samples of the CoPc solutions were taken all having equal volumes of 0.5 mL. For the calculation, the molar extinction coefficient of  $1.3 \pm 0.7 \times 10^5 \text{ L mol}^{-1}\text{cm}^{-1}$  was taken for the conventional solvents' high dissolving capacity to CoPc and used here for calculating the maximum saturation concentration of CoPc in DME-DOL solution. Accordingly, the Beer Lambert's equation,  $A_{\lambda_{max}} = \epsilon l C_{max}$  was employed to extract the  $C_{max}$ . Thus, the average maximum saturation concentration (solubility of CoPc) was found to be  $1.047 \times 10^{-6} \text{ mol L}^{-1}$ . Or it is calculated to be  $5.98 \times 10^{-3} \text{ g L}^{-1}$  based on the 0.005 L of solution considered. The UV spectra of the replicate CoPc samples are shown in the **Fig. S4**.

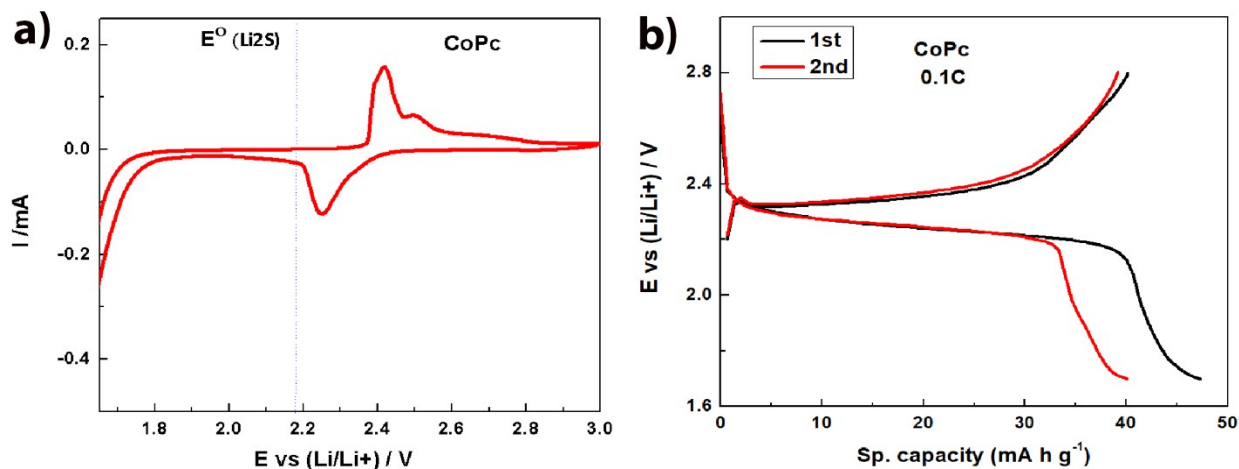


**Fig. S 6. a)** The CV profile of Cobalt Phthalocyanine/Super-P/Lithium cell (CoPc/Li-metal) with 0.5M LiTFSI electrolyte at scan rate of 0.1 mVs<sup>-1</sup>. **b)** The first two charge/discharge cycle profiles of the corresponding CoPc/Li-metal cell at 0.1C rate.

The electrochemical behavior of the CoPc was tested with cyclic voltammetry after fabricating the CoPc electrode mixed with the super-p carbon. As shown on the (**Fig.S6a**). The CV revealed a well-resolved reversible redox wave at 2.24 and 2.41V vs Li/Li<sup>+</sup> respectively for reduction and oxidation processes. The current response probably attributed to the electrochemical interconversion between Co(III) and Co (II) <sup>6</sup> together with corresponding insertion/de-insertion of Li<sup>+</sup> ion from the electrolyte. <sup>7</sup> The corresponding CoPc/Li-metal cell's charge/discharge cycle profiles are shown (**Fig.S6b**) in agreement with the CV curve. Hence, the CoPc, in addition to promoting the electrocatalytic conversion of sulfur and reduction products through electron transfer, the reversible redox conversion of CoPc accompanied with the Li<sup>+</sup> insertion/de-insertion during charging/discharging may contribute to capacity enhancement of the GN-CoPc-S cathode.

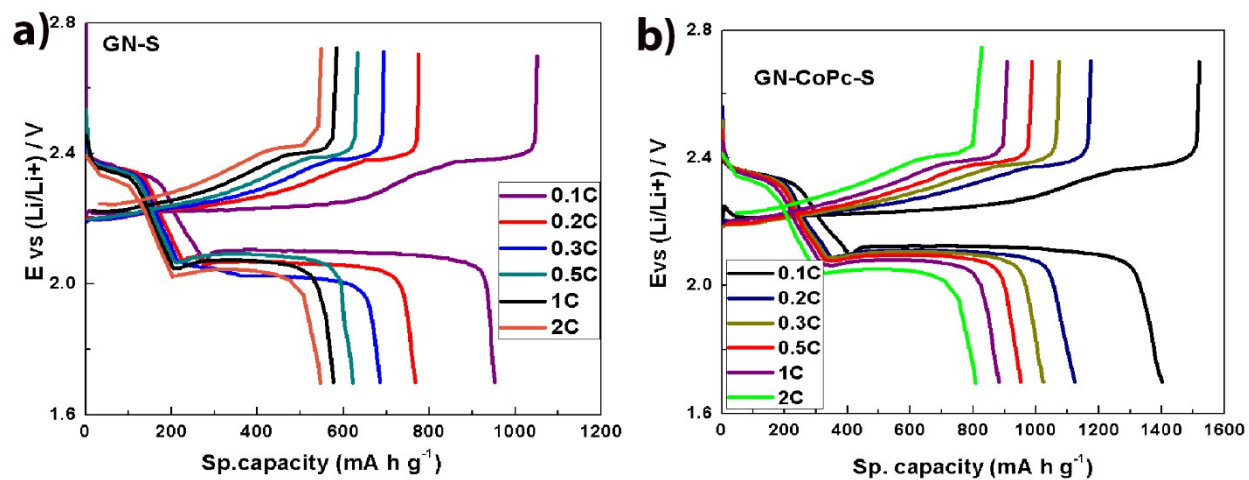
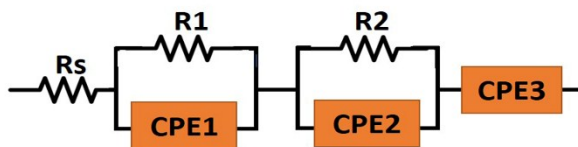
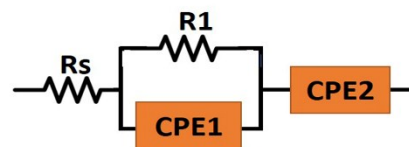


Fig. S 7. The Voltage profiles of Li-S cells at different C-rates: a) GN-S, b) GN-CoPc-S.

**a)**



**b)**



**Fig. S 8 a)** The EC-circuit model used to fit the EIS spectra of Li-S batteries with GN-CoPc-S and GN-S cathodes after 5<sup>th</sup> and 200<sup>th</sup> charge/discharge cycles. **b)** The EC-circuit model applied to fit the EIS spectra of the Li<sub>2</sub>S-CoPc-Super-p and Li<sub>2</sub>S-Super-P cathodes before and after activation cycle.

**Table S 1. FT-IR peak assignment for CoPc, GN, and GN-CoPc hybrid sample (refer Fig.1c in the main text).**

Sample Name	( $\nu = \text{cm}^{-1}$ )	Assignment	Ref.
CoPc	1469	beta (N-H) in plane bending	8
	1424	beta (C-H) vibration	8
	1330	C-C stretching in isoindole	9, 10
	1289	C-N stretching	9, 10
	1668	C=C macrocycle ring deformation	9, 10
	1119	C-N stretching	9, 10
	1093	C-N additional bonding	9
	911	Metal-N bond vibration	11
	758	gamma (C-H)	8
	732	C-H out of plane deformation of phenyl ring	9
GN	1469	skeletal vibration of GN sheet	12
	1439	C-O-C, C-O-H, C-O due to oxygen bridges	13 □ □ □ □ □ □
	1081	C-O bond stretching from the remaining carbonyl groups	14
	1041	C-O bond stretching from the remaining carbonyl groups	14
	960	C-O-C group	
	615	C-H bending	13 □ □ □ □ □ □
GN-CoPc	1469	skeletal vibration of GN sheet	12
	1439	C-O-C, C-O-H, C-O due to oxygen bridges	13 □ □ □ □ □ □
	1334	C-C stretching in isoindole	9, 10
	1286	C-N stretching	9, 10
	1081	C-O bond stretching from the remaining carbonyl groups	14
	1041	C-O bond stretching from the remaining carbonyl groups	14
	960	C-O-C group	
	733	C-H out of plane deformation of phenyl ring	9
	618	C-H bending	13 □ □ □ □ □ □

**Table S 2. C-rates and Corresponding over-potentials for Li-S batteries with GN-CoPc-S and GN-S cathodes determined from Fig.S7.**

C-Rate	0.1C	0.2C	0.3C	0.5C	1C	2C
GN-S ( $\Delta E$ )/mV	151	284	328	283	314	350
GN-CoPc-S ( $\Delta E$ )/mV	119	165	186	208	249	289

**Table S 3. The Resistance values extracted from the EIS spectra (refer Fig.2c&d in the main text) of the GN-CoPc-S and GN-S cathodes after 5<sup>th</sup> and 200<sup>th</sup> charge/discharge cycles, fitted using the EC-circuit model Fig. S8a.**

Li-S Cell	<b>Rs(Ω)</b>	<b>R1(Ω)</b>	<b>R2(Ω)</b>
GN-S (5th)	16.39	31.52	19.97
GN-CoPc-S (5th)	16.51	14.62	5.62
GN-S (200th)	16.92	47.03	49.99
GN-CoPc-S (200th)	16.03	28.93	13.36

Where, **Rs**, **R1** and **R2** represent the electrolyte (solution), electrode-solution and charge transfer resistances respectively of EC-circuit given **Fig.S8a**. Constant phase element (CPE) is used instead of pure capacitances and the Warburg element to compensate the non-ideality of the electrodes during modeling of the electrochemical cells. Therefore, **CPE1** and **CPE2** represent the capacitance of the two semi-circles at high and medium frequency respectively and the **CPE3** stands for the Warburg line at low frequency region.

**Table S 4. The Resistance values extracted from the EIS spectra (refer Fig.5a&c in main text) of the Li<sub>2</sub>S-Super-P and Li<sub>2</sub>S-CoPc-Super-P cathodes before and after activation, fitted using the EC-circuit model Fig. S8b.**

Li <sub>2</sub> S-Cell	<b>Rs (Ω)</b>	<b>R1(Ω)</b>
Li <sub>2</sub> S-Super-P (Before)	2.68	352.60
Li <sub>2</sub> S-CoPc-Super-P (Before)	2.79	80.76
Li <sub>2</sub> S-Super-P (After)	1.51	1005
Li <sub>2</sub> S-CoPc-Super-P (After)	1.54	50.59

Where, **Rs** and **R1** represent the electrolyte (solution) and charge transfer resistances respectively; while **CPE1** designate the capacitance of the semi-circle and **CPE2** the Warburg line at a low-frequency region in the case of EC-circuit **Fig.S8b**.

## References

1. L. N. Ramavathu, K. K. Maniam, K. Gopalram and R. Chetty, *J. Appl. Electrochem.*, 2012, **42**, 945-951.
2. K. Pawan, K. Arvind, S. Bojja, S. Bir, S. R. Siddharth and L. J. Suman, *Chem. Eur. J.*, 2014, **20**, 6154-6161.
3. W. B. B. Cicero, Z. Lei, L. Kunchan, L. Hansan, L. B. M. Aldaléa, P. M. Edmar, W. Haijiang and Z. Jiujun, *Electrochim. Acta*, 2008, **53**, 4937-4951.
4. Y. Lu and R. G. Reddy, *Electrochim. Acta*, 2007, **52**, 2562-2569.
5. F. Ghani, J. Kristen and H. Riegler, *JCED*, 2012, **57**, 439-449.
6. K. I. Ozoemena and T. Nyokong, *Electrochim. Acta*, 2006, **51**, 2669-2677.
7. T. Brousse, D. Be' langer and J. W. Long, *J. Electrochem. Soc.*, 2015, **162**, A5185-A5189.
8. N. Mhadhbi, S. Saïd, S. Elleuch and H. Naïli, *J. Mol. Struct.*, 2016, **1108**, 223-234.
9. B. B. Topuz, G. Gündüz, B. Mavis and Ü. Çolak, *Dyes Pigm.*, 2013, **96**, 31-37.
10. M. Mukherjee, U. K. Ghorai, M. Samanta, A. Santra, G. P. Das and K. K. Chattopadhyay, *Appl. Surf. Sci.*, 2017, **418**, 156-162.
11. T. Kobayashi, F. Kurokawa, N. Uyeda and E. Suito, *Spectrochim. Acta, Part A*, 1970, **26**, 1305-1311.
12. C. H. Manoratne, S. R. D. Rosa and I. R. M. Kottegoda, *Mater. Sci. Res. India*, 2017, **14**, 19-30.
13. M. Hayyan, A. Abo-Hamad, M. A. AlSaadi and M. Ali Hashim, *Nanoscale Res. Lett.*, 2015, **10**, 1004-1030 □.□□□□□□
14. F. T. Thema, M. J. Moloto, E. D. Dikio, N. N. Nyangiwe, L. Kotsedi, M. Maaza and M. Khenfouch, *J. Chem.*, 2013, 1-6.